Molecular Therapy
Methods & Clinical Development
Original Article

A Direct Comparison of IV and ICV Delivery Methods for Gene Replacement Therapy in a Mouse Model of SMARD1

Monir Shababi,[1,2,7] Eric Villalón,[1,2,6] Kevin A. Kaifer,[1,2,6] Vince DeMarco,[3,4,5] and Christian L. Lorson[1,2,7]

[1]Department of Veterinary Pathobiology, College of Veterinary Medicine, University of Missouri, Columbia, MO, USA; [2]Bond Life Sciences Center, University of Missouri, Columbia, MO, USA; [3]Department of Medicine, Division of Endocrinology, Diabetes and Cardiovascular Center, University of Missouri, Columbia, MO, USA; [4]Department of Medical Pharmacology and Physiology, School of Medicine, University of Missouri, Columbia, MO, USA; [5]Research Service, Harry S. Truman Memorial Veterans Hospital, University of Missouri, Columbia, MO, USA

Spinal muscular atrophy with respiratory distress type 1 (SMARD1) is an infantile autosomal recessive disease caused by the loss of the ubiquitously expressed *IGHMBP2* gene. SMARD1 causes degeneration of alpha-motor neurons, resulting in distal muscle weakness, diaphragm paralysis, and respiratory malfunction. We have reported that delivery of a low dose of AAV9-*IGHMBP2* to the CNS results in a significant rescue of the SMARD1 mouse model (*nmd*). To examine how a delivery route can impact efficacy, a direct comparison of intravenous (IV) and intracerebroventricular (ICV) delivery of AAV9-*IGHMBP2* was performed. Using a low-dose, both IV and ICV delivery routes led to a significant extension in survival and increased body weight. Conversely, only ICV-treated animals demonstrated improvements in the hindlimb muscle, neuromuscular junction, and motor function. The hindlimb phenotype of IV-treated mice resembled the untreated *nmd* mice. We investigated whether the increased survival of IV-treated *nmd* mice was the result of a positive impact on the cardiac function. Our results revealed that cardiac function and pathology were similarly improved in IV- and ICV-treated mice. We concluded that while IV delivery of a low dose does not improve the hindlimb phenotype and motor function, partial restoration of cardiac performance is sufficient to significantly extend survival.

INTRODUCTION

Spinal muscular atrophy with respiratory distress type 1 (SMARD1) is an autosomal recessive motor neuron disease that is initially characterized by early distal lower limb muscle atrophy following proximal muscle weakness.[1,2] Unlike 5q spinal muscular atrophy, in which intercostal muscle atrophy results in respiratory complications, SMARD1 patients exhibit diaphragmatic paralysis between 6 weeks and 13 months of age, leading to fatal respiratory malfunction.[1,3,4] The gene responsible for SMARD1 development is *immunoglobulin μ-binding protein 2* (*IGHMBP2*). The IGHMPB2 protein has been classified as a member of the Upf1-like group within the helicase superfamily1 (SF1), consisting of the helicase domain, the R3H domain, the zinc finger domain, and the nuclear localization signal sequence.[5] The majority of the patient mutations cluster within the helicase domain and are missense mutations.[3,6,7] IGHMBP2 is ubiquitously expressed and comprises 15 exons encoding 993 amino acids corresponding to an ~110 kDa product. The exact role of IGHMBP2 linking to disease development is unknown; however, several cellular activities have been ascribed to the normal protein, including ribosomal RNA maturation and translation,[8,9] immunoglobulin-class switching,[7] pre-mRNA maturation,[10] and transcription regulation by either DNA binding activity[11,12] or interaction with TATA-binding protein.[13]

The human and mouse *IGHMBP2* genes are highly homologous. The genetic basis for the most frequently utilized mouse model of SMARD1 is derived from a spontaneous mutation in the previously described *nmd* mice.[14] *nmd* mice contain a mutation in *Ighmbp2* intron 4, and, while a corresponding patient mutation does not exist, this mutation disrupts the normal splicing pattern of the *Ighmbp2* transcript,[14,15] causing aberrant splicing of ~75%–80% of the *Ighmbp2*-derived mRNAs.[14,16] The lifespan of *nmd* mice is variable, ranging from 10 weeks to 7 months.[14,17,18] A hallmark of the *nmd* phenotype includes hindlimb muscle weakness and retrenchment that appears within the second week of age and progresses to the forelimb and trunk muscles.[16,18] While cardiomyopathy is rarely reported in SMARD1 patients, it is a consistent phenotype observed in *nmd* mice. Functional and structural cardiac defects can be rescued by cardiac-specific restoration of *Ighmbp2* expression in *nmd* mice.[19] In contrast, neuronal-specific expression of *Ighmbp2* only results in motor function rescue and fails to alleviate the cardiomyopathy, leading to death from congestive heart failure.[20] Consistent with this, simultaneous restoration of *Ighmbp2* in the neurons and skeletal muscle of

Received 8 July 2018; accepted 13 August 2018;
https://doi.org/10.1016/j.omtm.2018.08.005.

[6]These authors contributed equally to this work.

[7]Senior author

Correspondence: Monir Shababi, PhD, Bond Life Sciences Center, Room 404, University of Missouri, Columbia, MO 65211, USA.
E-mail: shababim@missouri.edu

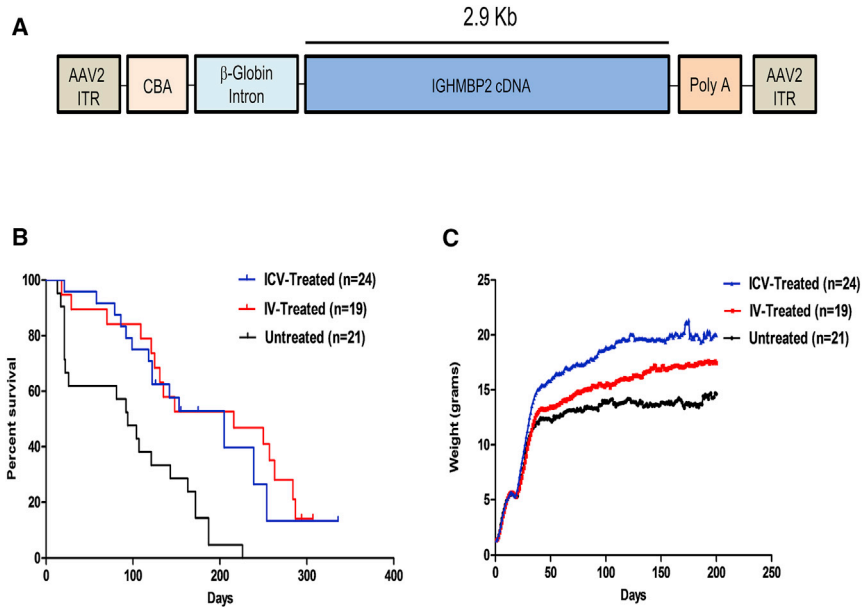

Figure 1. ICV and IV Injection of AAV9-*IGHMBP2* in Low Doses Significantly Increases the Survival and Total Body Weight of *nmd* Mice

(A) Map of AAV9-*IGHMBP2* containing 2.9 kb of human *IGHMBP2* cDNA under control of the ubiquitously expressing *chicken-beta-actin* (CBA) promoter along with an optimized intron within the 5′ leader sequence and a synthetic polyA site cloned into a single-stranded AAV vector. (B) Homozygous *nmd* mice were injected either ICV (at P2 and P3) or IV at P2 with a low dose (1.25×10^{11}) of genomic copies of AAV9-*IGHMBP2* and compared to untreated mice. Survival was determined by Kaplan-Meier curves, and the p value was determined by the log-rank (Mantel-Cox) test. Median survival of ICV-injected *nmd* mice (n = 24) was 205 days and IV-injected (n = 19) 216 days compared to 94 days in untreated *nmd* mice (n = 21) ($p = 0.0006$). Median survival of IV- and ICV-injected *nmd* mice was not significant ($p = 0.995$). (C) Weight assessment of ICV- and IV-treated *nmd* mice compared to untreated mice. The average weight of ICV-treated *nmd* mice is 16.63 ± 0.33 g compared to 12.24 ± 0.21 g in untreated mice (one-way ANOVA $p < 0.001$) and 14.09 ± 0.28 g in IV-treated mice (one-way ANOVA $p < 0.05$). The average weight of IV-treated animals is significantly higher than untreated *nmd* animals (one-way ANOVA $p < 0.01$).

nmd mice leads to complete rescue.[19] These observations highlight the differences between the research model and the clinical cases, but also the necessity of efficient cardiac rescue for the success of any therapeutic strategy in *nmd* mice.

There is currently no cure or effective therapy for SMARD1. Recently, we and another group developed the gene replacement therapy for this monogenic disease.[18,21] These reports contain vector-based approaches to rescue the *nmd* phenotype by delivering adeno-associated virus serotype 9 (AAV9) expressing the full-length human *IGHMBP2* cDNA into the CNS using two different doses[18] and systemically using a high dose.[21] To further advance AAV9-*IGHMBP2* therapy, it is important to determine the most appropriate dose coupled with the most efficient delivery. To investigate an optimized delivery paradigm, a relatively low dose of AAV9-*IGHMBP2* virus was used in this study to allow differences to be observed between various routes of administration. In this article, we provide evidence that intravenous (IV) delivery of a low dose of AAV9-*IGHMBP2* significantly improves the survival and cardiac phenotype of *nmd* mice but is less effective at restoring the hindlimb phenotype and motor function. We conclude that cardiac rescue in *nmd* mice is sufficient to extend the survival of the IV-treated animals and the efficacy of AAV9-*IGHMPB2* is impacted by the route of delivery.

RESULTS

Phenotypic Assessment of IV- and ICV-Treated *nmd* Mice

The previously described viral vector utilized in the subsequent experiments expresses the full-length human *IGHMBP2* cDNA (Figure 1A).[18] To directly compare the efficiency of two different delivery methods, we performed phenotypic analysis using a low dose (1.25e11 vector genomes [vg]) of single-stranded AAV9-*IGHMBP2* delivered on postnatal day 2 (P2) either through intracerebroventricular (ICV) or IV injection via the facial vein. This dose was effective in rescuing the *nmd* phenotype by ICV injection.[18] Interestingly, both IV and ICV delivery routes led to a similar extension in survival ($p = 0.995$; 216 days median survival for IV-treated compared to 205 days for ICV-treated mice) (Figure 1B). The extension in survival for IV- and ICV-treated animals was significantly higher than untreated animals ($p = 0.0006$; 94 days median survival for untreated animals) (Figure 1B). Consistent with increased lifespan, both IV- and ICV-treated animals gained considerably more weight than untreated animals ($p < 0.0001$); however, the ICV-treated cohort gained significantly more weight than the IV-treated cohort ($p < 0.0001$) (Figure 1C). As anticipated, treated males from both groups gained more weight than treated females, consistent with our previously published results.[18]

One of the hallmarks of the *nmd* phenotype is a severe contracture in the hindlimb, but the ability to splay the hindlimb is significantly improved in ICV-treated *nmd* mice.[18] To compare the relative degree of rescue in the hindlimb contracture phenotype, each cohort was analyzed in a "tube test" and a tail suspension test (Figures 2A and 2C). Even though IV-treated *nmd* mice displayed rescue in the contracture phenotype compared to untreated animals (Figures 2A and 2B), ICV-treated mice showed a greater improvement compared to the IV-treated cohort ($p < 0.0001$) (Figures 2A–2C). ICV-treated and unaffected control mice were very similar regarding their hindlimb phenotype (Figures 2A–2C). In addition, rotarod and grip strength tests were performed to assess motor function in each of the cohorts starting at P50 for 7 alternating days and/or trials. Motor

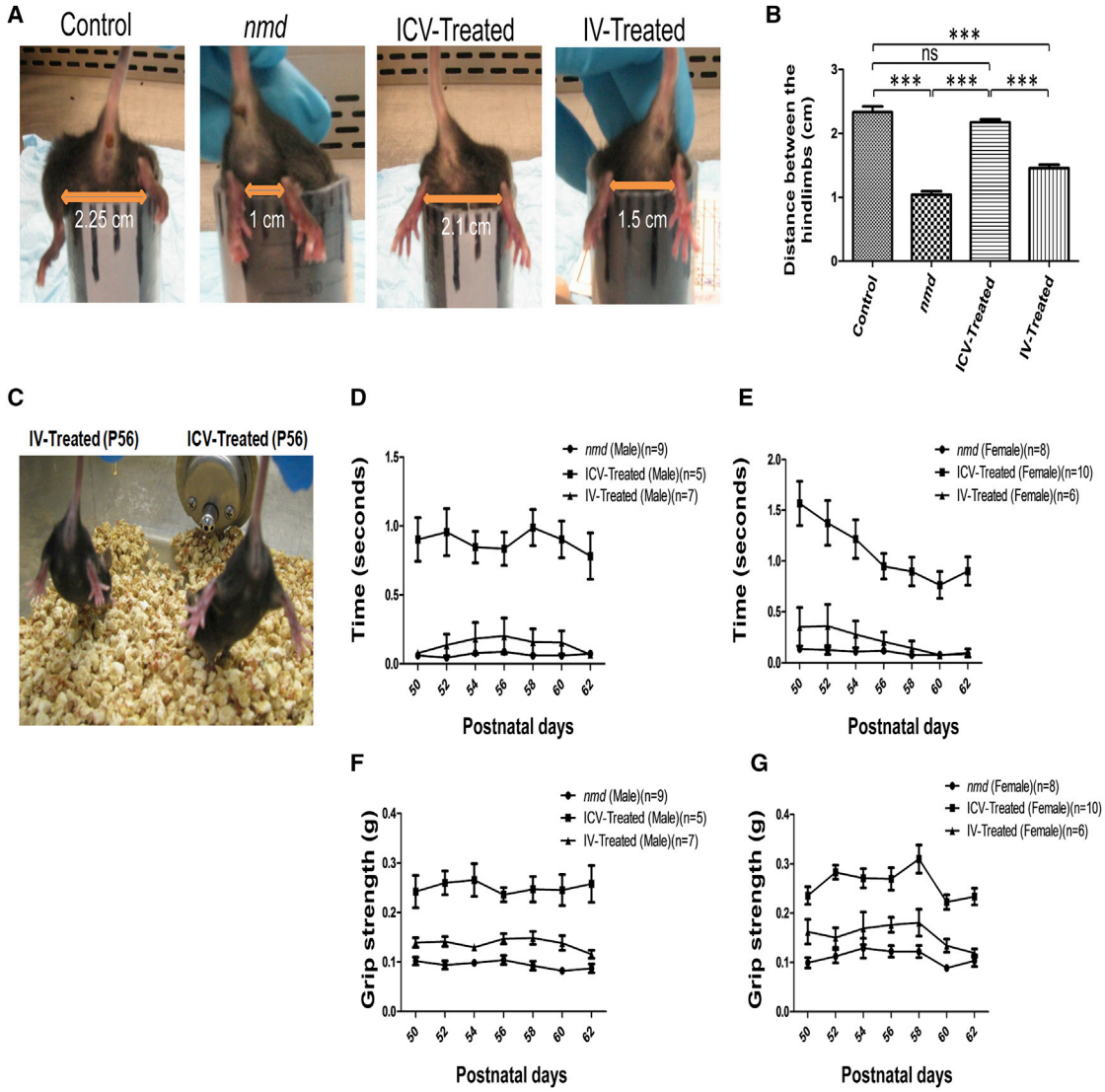

Figure 2. The Hindlimb Contracture and Motor Function of IV-Treated *nmd* Mice Are Not Rescued Compared to ICV-Treated Mice

(A) Heterozygous (control) and homozygous *nmd* mice (untreated, IV-treated, and ICV-treated) were tested for hindlimb suspension by placing them upside down from a conical tube. Hanging from the tube, the length of separation between their hindlimbs was analyzed and measured on 3 consecutive days. (B) The degree of the hindlimb splay did not differ statistically in the control and ICV-treated *nmd* mice, whereas the hindlimb contracture was still significantly impaired in IV-treated mice (one-way ANOVA IV-treated versus ICV-treated, $p < 0.001$). (C) Suspended from the tail, all of the IV-treated *nmd* mice show severe hindlimb contracture compared with age-matched ICV-treated mice, which shows rescued hindlimb phenotype (photo taken at P56). (D and E) Rotarod performance was used to measure riding time parameter in seconds; IV- and ICV-treated *nmd* males (D) and females (E) were compared with the times of their age-matched untreated *nmd* littermates; rotarod statistical significance was identical for both males and females (one-way ANOVA, ICV versus IV and untreated $p < 0.001$; IV versus untreated, ns). (F and G) Grip strength measurements in grams; IV- and ICV-treated *nmd* males (F) and females (G) were compared with their age-matched untreated *nmd* counterparts (one way ANOVA, ICV- versus IV-treated [females], $p < 0.01$; ICV- versus IV-treated [males], $p < 0.001$; IV versus untreated [females], ns; IV versus untreated [males], $p < 0.05$). The data were normalized to the times (rotarod) and gram (grip strength) of the heterozygous control and graphed as the ratio of the control value. Measurements were taken on alternative days from P50 through P62. Error bars represent ± SEM. ***$p < 0.001$.

function results were normalized to unaffected control cohorts and graphed based on gender, which confirmed both genders were performing similarly. Consistent with the hindlimb contracture studies, the rotarod performance of the ICV-treated animals was indistinguishable from the unaffected control group and was significantly improved compared to IV-treated mice (ICV versus IV, $p < 0.0001$) (Figures 2D and 2E). Rotarod performance of IV-treated animals was similar to untreated littermates ($p = 0.34$) (Figures 2D and 2E). In the grip strength analysis, ICV-treated animals were significantly weaker than unaffected mice but were still drastically improved

compared to the IV-treated cohort (ICV compared to IV, $p < 0.0001$) (Figures 2F and 2G). In contrast to the rotarod results, the grip strength test of IV-treated mice revealed that males had more strength than the female cohort (IV males versus untreated males, $p < 0.05$; IV females compared to untreated females, ns) (Figures 2F and 2G). Collectively, these results demonstrate that the survival of IV- and ICV-treated animals is equally extended, although ICV-treatment significantly improves additional aspects of the *nmd* phenotype, including weight, motor function, and hindlimb contracture.

Hindlimb Muscle and Neuromuscular Junction Pathology Is Not Rescued in IV-Treated *nmd* Mice

To determine whether skeletal muscle pathology was differentially affected in the IV- and ICV-treated groups, a muscle fiber cross-sectional area and the degree of interstitial fibrosis were examined in gastrocnemius muscles. To maintain consistency throughout the experiments, tissues were collected from 8-week-old males of unaffected control, untreated, and ICV- and IV-treated *nmd* mice and examined by using Verhoeff-van Gieson (VVG) staining (Figure 3A). Consistent with previous reports, untreated *nmd* muscles displayed fiber atrophy, highly variant fiber size, centralized nuclei, and interstitial and periarterial fibrosis (Figure 3A).[18,21,22] As anticipated, the typical *nmd*-associated pathology was significantly reduced in the ICV-treated samples, as no significant difference was observed between unaffected and ICV-treated mice (Figures 3A–3C). In contrast, muscle from the IV-injected samples displayed significant levels of pathology (ICV versus IV, $p < 0.0001$) and were similar to untreated *nmd* samples in regards to fiber size and intensity of fibrosis (Figures 3A–3C). These results further proved that ICV delivery of AAV9-*IGHMBP2* resulted in greater rescue of the *nmd* phenotype and that IV delivery had no positive impact on the gastrocnemius muscle pathology, providing a basis for the differential efficacy with respect to hindlimb contracture and rotarod performance.

Due to lack of improvements in the gastrocnemius muscles of IV-treated *nmd* mice, it was anticipated that their neuromuscular junctions (NMJs) innervating the gastrocnemius would also exhibit more of the *nmd* phenotype compared to ICV-treated samples. In a blinded, quantitative assessment of NMJ pathology from the gastrocnemius, IV-treated NMJs exhibited the hallmark pattern of neurodegeneration, including nearly 90% denervated and fragmented endplates (Figures 3D–3F). In contrast, NMJs from ICV-treated samples were significantly rescued, as only 30% of the NMJs were denervated, compared to NMJs from unaffected mice, which showed no detectable denervation or motor endplate fragmentation (Figures 3D–3F). The NMJ phenotype of IV-treated mice is consistent with the hindlimb muscle pathology and motor function tests, providing further evidence that IV delivery of a low dose of AAV9-*IGHMBP2* does not efficiently rescue the disease phenotype in distal muscles.

Diaphragm Muscle Pathology Is Similarly Rescued in IV- and ICV-Treated *nmd* Mice

Diaphragm muscles of *nmd* mice exhibit pathology at 8 and 14 weeks of age.[18,22] To determine whether IV and ICV delivery of low-dose vector similarly impact disease progression, we compared the VVG-stained cross sections of diaphragm muscles from each cohort. As expected, the *nmd* diaphragm showed areas of hypertrophy as well as regions comprised of small and degenerated fibers in addition to fibrotic areas (Figures 4A and 4C). In contrast to untreated *nmd* tissue, the irregular fiber size and fibrosis were drastically decreased in IV- and ICV-treated diaphragms, representing a phenotype similar to the unaffected control (Figures 4A–4D). In contrast to distal muscles, low dose administration of AAV9-*IGHMBP2* significantly repaired diaphragm pathology independent of the route of administration.

Cardiomyocytes from IV- and ICV-Treated Animals Are Similarly Rescued

Since *nmd* mice develop cardiomyopathy, cardiac-specific transgenic restoration of *Ighmbp2* can extend survival.[19] To determine whether IV and ICV delivery of AAV9-*IGHBMP2* differentially rescued the cardiac phenotype in *nmd* mice, we analyzed images from wheat germ agglutinin (WGA)- and VVG-stained heart sections in each of the cohorts. As expected, cardiomyocytes from *nmd* mice exhibited the pathological hallmarks of cardiomyopathy, including smaller fibers accompanied by areas of hypertrophy, myocyte nuclear enlargements, unorganized and degenerated muscle fibers, and interstitial and periarterial fibrosis, evidenced by accumulation of collagen (pink areas in VVG staining) (Figures 5A and 5C). Quantification of the cardiomyocyte cross-sectional area in WGA staining demonstrated that unaffected controls are not statistically different than untreated or treated *nmd* mice. However, the untreated fibers are generally smaller, while ICV- and IV-treated hearts exhibit a minor hypertrophy (Figures 5A and 5B), leading to a notable difference only between ICV-treated and untreated hearts ($p < 0.05$). In regard to fibrosis, both delivery methods resulted in significantly reduced levels of fibrosis in the heart tissue compared to untreated *nmd* (Figures 5C and 5D).

The Underlying Cause of Interstitial and Periarterial Fibrosis Is Equally Diminished in IV- and ICV-Treated *nmd* Hearts

Interstitial and periarterial fibrosis occurs as a result of excess extracellular matrix (ECM) proteins in cardiomyocytes and the arterial wall. A balanced synthesis of the ECM proteins is influenced by the proper level of growth factors and cytokines produced by cardiac fibroblasts.[23–26] To examine potential defects in ECM protein expression, collagen I and collagen III expression was analyzed by immunohistochemistry in cardiomyocytes and the arterial wall (Figures 6A–6C). Collagen type I was significantly higher in the cardiomyocytes of untreated *nmd* mice compared to unaffected control and ICV- and IV-treated mice (Figures 6A and 6F). In contrast, collagen III expression and the ratio of collagen III/I was significantly reduced in the arteries of untreated and IV- and ICV-treated mice compared to unaffected controls (Figures 6B, 6C, 6G, 6H, and S1A). These results suggest that high expression of collagen I contributes to interstitial fibrosis in *nmd* cardiomyocytes, which is rescued by both delivery methods. However, the untreated group and both of the

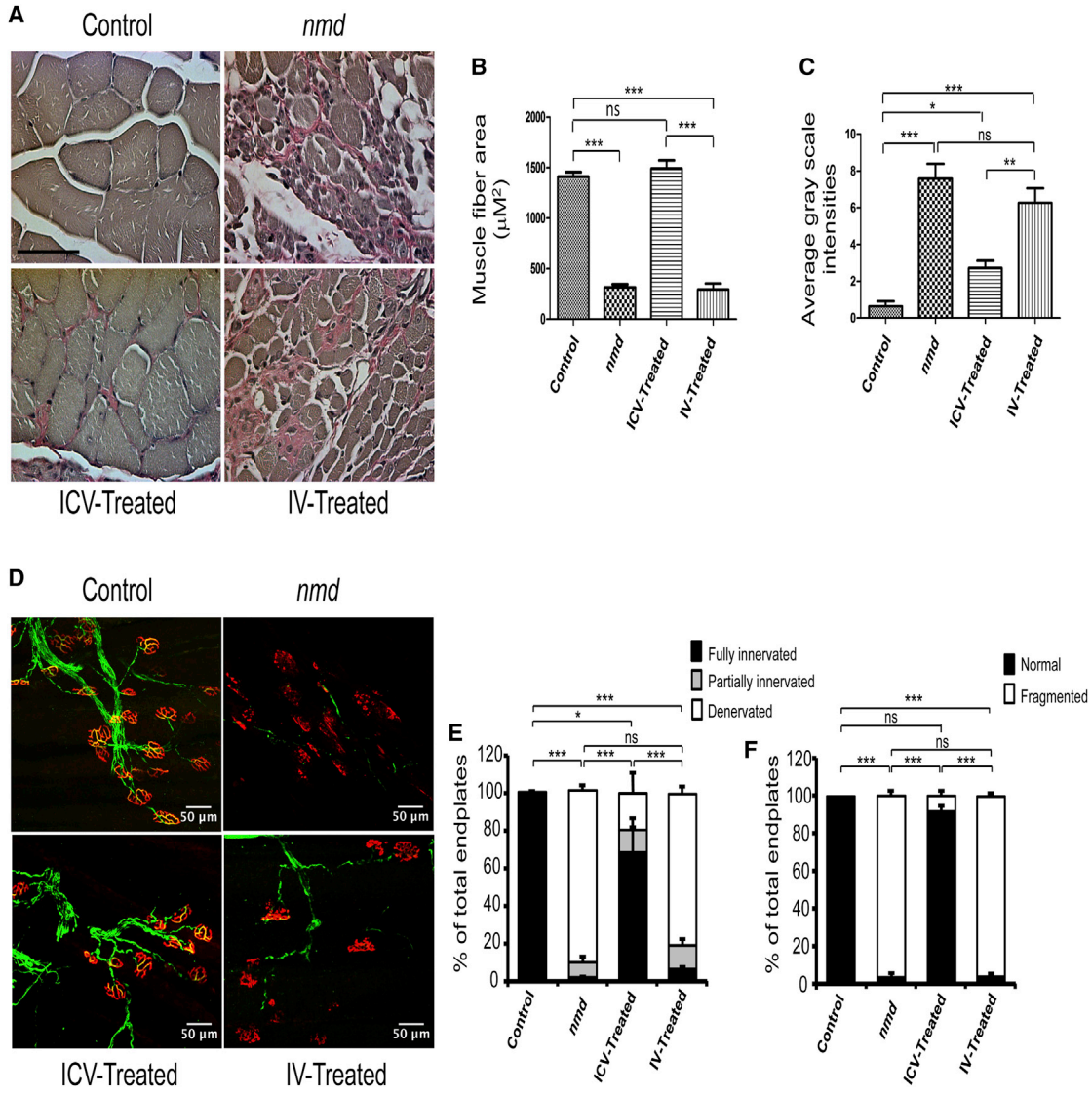

Figure 3. Gastrocnemius Muscle and NMJ Defects Are not Rescued in IV-Treated *nmd* Mice Compared to ICV-Treated Mice

(A) VVG-stained cross sections of gastrocnemius muscles of IV- and ICV-treated *nmd* males were examined at 8 weeks post-injection under 40× magnifications and compared with those of age-matched untreated *nmd* and healthy control mice (n = 4 for each group). (B) The area size of muscle fiber in IV-treated *nmd* mice is similar to untreated mice and significantly reduced compared to ICV-treated mice (one-way ANOVA, IV versus ICV, $p < 0.001$). (C) The intensity of interstitial and periarterial fibrosis is significantly higher in the muscles of IV-treated *nmd* mice compared to ICV-treated (one way ANOVA $p < 0.01$) and unaffected control mice (one-way ANOVA, $p < 0.001$). (D) NMJs from gastrocnemius muscle of IV- and ICV-treated males at 8 weeks of age compared to those of age-matched untreated and healthy control (n = 4 for each group). Muscles were labeled with α-BTX for acetylcholine receptors (AChRs), anti-neurofilament, and anti-vesicular acetylcholine transporter (VAChT) for nerve terminals. (E) Percentage of innervated, partially innervated, and denervated muscles; % of fully innervated in ICV-treated is ~69% versus ~7% in IV-treated mice (one-way ANOVA, $p < 0.001$). (F) Percentage of fragmented endplates in ICV-treated is ~8% versus ~96% in IV-treated mice (one-way ANOVA, $p < 0.001$). Scale bars, 50 μm. Error bars represent mean ± SEM. *$p < 0.05$ and ***$p < 0.001$.

treated groups are susceptible to vascular rupture as a result of reduced collagen III and an imbalanced collagen III/I ratio in arteries.

To investigate whether other ECM proteins contribute to periarterial fibrosis, arterial walls were examined for the potential deposition of fibronectin. Interestingly, a significant increase in fibronectin deposition was detected in the adventitia of untreated *nmd* samples. In contrast, fibronectin levels in IV- and ICV-treated arteries were similar to unaffected control (Figures 6D and 6I), suggesting fibronectin deposition is a potential factor in the development of periarterial fibrosis in *nmd*.

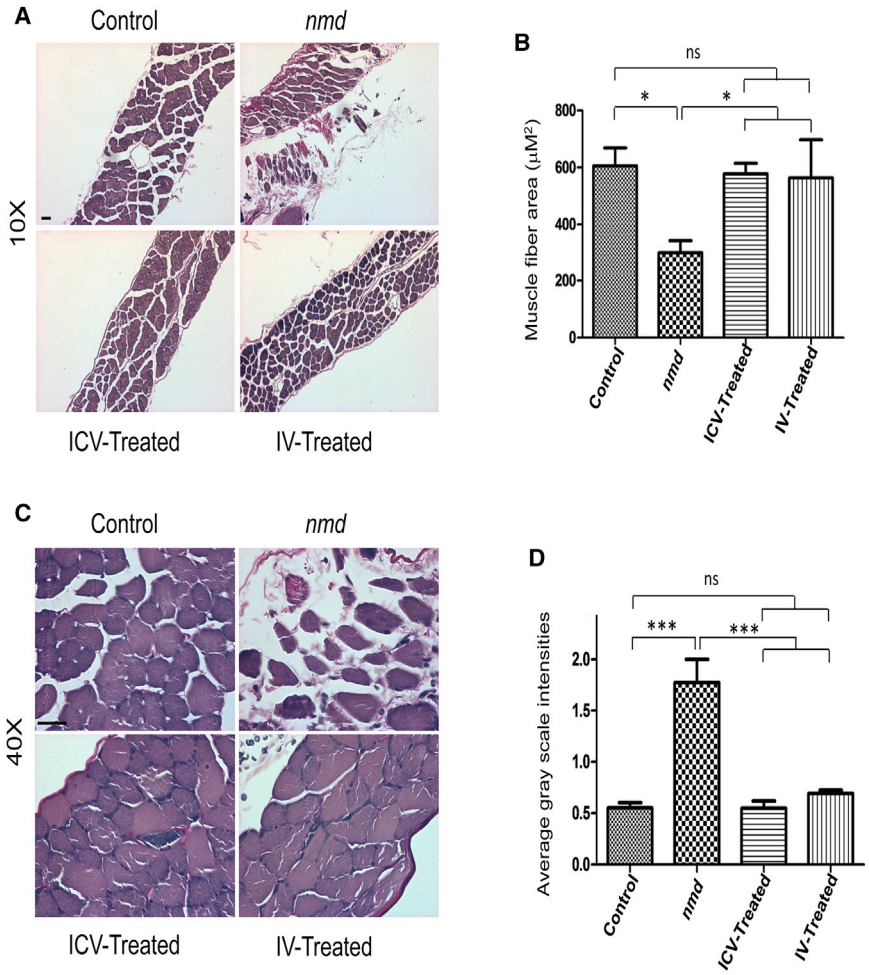

Figure 4. Diaphragm Muscle Pathology of IV- and ICV-Treated *nmd* Mice Is Equally Repaired Compared to Untreated Mice

(A and C) VVG-stained cross sections of diaphragm muscles of IV- and ICV-treated males were examined at 8 weeks post-injection under 10× (A) and 40× (C) magnifications and compared with those of age-matched untreated *nmd* and healthy control (n = 4 for each group). (B) The area size of muscle fiber in both IV- and ICV-treated *nmd* mice is significantly increased compared to untreated mice (one-way ANOVA, $p < 0.05$). (D) The intensity of interstitial and periarterial fibrosis is significantly decreased in diaphragm muscles of IV- and ICV-treated *nmd* mice compared to untreated mice (one-way ANOVA, $p < 0.001$). Error bars represent mean ± SEM. Scale bars, 50 μm. *$p < 0.05$ and ***$p < 0.001$.

To determine the underlying cause of fibrosis in the *nmd* heart, we focused on two pleiotropic growth factors, transforming growth factor β1 (TGFβ1) and connective tissue growth factor (CTGF), which play a role in the development of fibrosis by increasing the synthesis of the ECM proteins. Additionally, CTGF is a key mediator of ECM production in pathological fibrotic conditions, cardiac hypertrophy, and heart failure.[24,27–29] We observed a significantly higher expression of CTGF in untreated cardiomyocytes and arteries compared to healthy control and IV- and ICV-treated animals (Figures 6E, 6J, and S1B). In contrast, TGFβ1 levels in the cardiomyocytes and arteries are not significantly different between any of the cohorts (Figures S1C and S1D), suggesting that TGFβ1 is not a causative factor in imbalanced ECM synthesis in the *nmd* heart.

Collectively, the hearts of IV- and ICV-treated *nmd* mice developed considerably less fibrotic area compared to untreated mice, indicated by a lower expression of ECM proteins such as collagen I and fibronectin. One of the underlying causes of fibrosis in *nmd* hearts is the upregulation of CTGF, which is notably rescued in both ICV- and IV-treated cardiomyocytes and arteries. However, decreased intensity of collagen III and, therefore, a reduced ratio of collagen III/I, was not salvaged in IV- and ICV-treated arteries, which places them alongside untreated *nmd* mice at high risk for arterial rupture.

Cardiac Ultrasound Reveals Moderate Rescue in Cardiac Function of Both IV- and ICV-Treated *nmd* Mice

To conduct measurements of cardiac function, echocardiography was performed on 8-week-old sedated mice. *nmd* mice develop cardiomyopathy within 4–6 weeks of age and, by 8 weeks, their cardiac function is severely compromised.[19] Due to their weak heart, 3 untreated *nmd* mice died soon after being anesthetized with isoflurane. As a result, the untreated mice with healthier hearts were unintentionally selected for cardiac ultrasound. We included both healthy controls (wild-type and unaffected heterozygous) for comparison to detect even moderate improvements in the treated hearts in case they resembled the heterozygous ("HET") more than the wild-type. We determined several cardiac functional parameters, including (1) left ventricular (LV) ejection fraction; (2) cardiac output; (3) LV diastolic function; (4) LV filling pressure; (5) diastolic stiffness; and (6) the LA/AO ratio based on the diameter of aorta (AO) and lumen (LA). As expected, *nmd* mice demonstrated insufficient cardiac systolic function, indicated by decreased ejection fraction and cardiac output (Figures 7A and 7B) as well as impaired LV diastolic function evidenced by reduced septal annular velocity (E'), increased LV filling pressure (E/E'), and increased diastolic stiffness estimated by the ratio of LV filling pressure (E/E') to LV inner diameter at end diastole (LVIDd) (Figures 7C–7E). The slight increase in the left atrial to aorta diameter ratio in untreated is consistent with remodeling resulting from the increase in LV filling pressure (Figures 7F, S2A, and S2B).

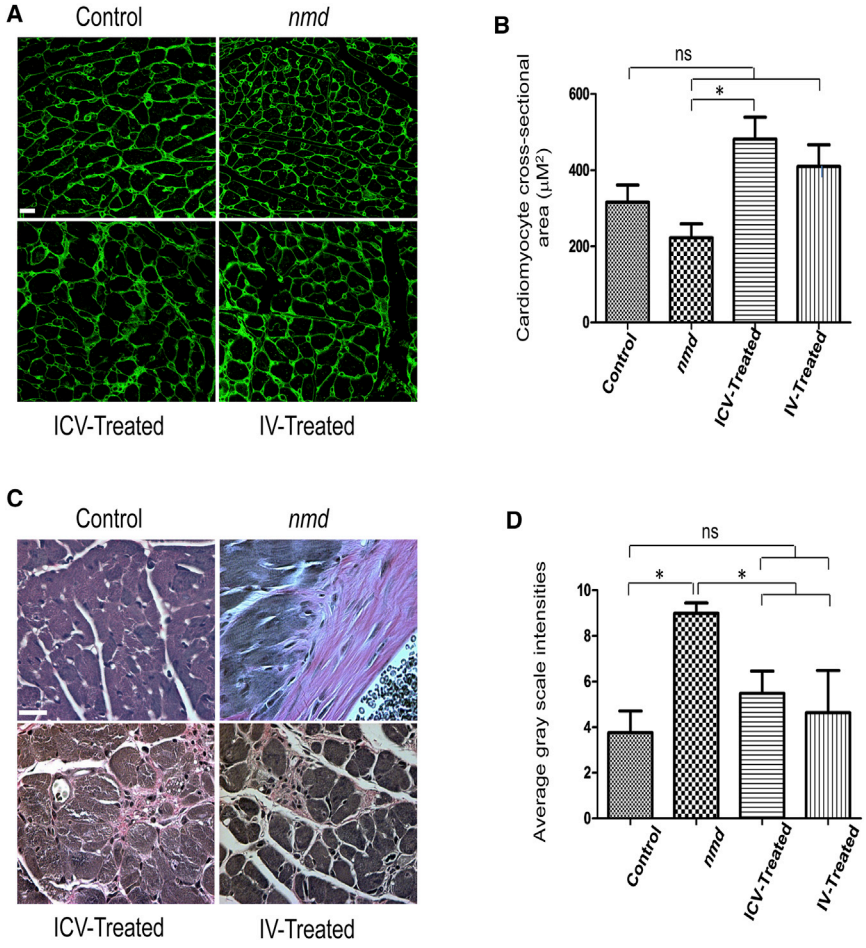

Figure 5. Cardiomyocyte Pathology of IV- and ICV-Treated *nmd* Mice Is Equally Repaired Compared to Untreated Mice

WGA-stained (A) and VVG-stained (C) cross sections of cardiomyocyte of IV- and ICV-treated males were examined at 8 weeks post-injection and compared with those of age-matched untreated *nmd* and healthy control males (n = 4 for each group). (A and B) The fiber area of cardiomyocytes in untreated *nmd* is slightly smaller than IV and healthy control but significantly decreased compared to ICV-treated *nmd* mice (one-way ANOVA, $p < 0.05$). The cardiomyocyte fiber area of IV, ICV, and healthy control are not statistically different. (C and D) The intensity of interstitial and periarterial fibrosis is significantly decreased in the cardiomyocytes of IV- and ICV-treated *nmd* mice compared to untreated mice (one-way ANOVA, $p < 0.05$). Error bars represent mean ± SEM. Scale bars, 50 μm. *$p < 0.05$

Accordingly, the myocardial performance index (marker of global cardiac dysfunction based on systolic and diastolic time intervals) was also elevated in untreated compared to healthy controls (Figure S2C). IV- and ICV-injected animals differed in some aspects of diastolic function, as LV filling pressure was more improved in IV-treated compared to ICV-treated mice (Figure 7D), and, therefore, LV diastolic function and the diastolic stiffness were rescued more efficiently in IV- than ICV-treated mice (Figures 7C and 7E). In contrast to the well-described cardiac phenotype of spinal muscular atrophy (SMA) mice in which bradycardia is a prominent defect,[30–32] the heart rate of *nmd* mice was similar between all groups (Figure S2D).

Collectively, the majority of the cardiac parameters were equally repaired in both IV- and ICV-treated mice to levels that were significantly more improved than untreated mice and did not differ statistically from their wild-type and "HET" counterparts (Figures 7A–7E). These data demonstrate that repair in cardiac function of IV- and ICV-treated hearts correlates with the rescue in cellular and biochemical properties of cardiomyocytes and arteries.

Levels of IGHMBP2 in the *nmd* Spinal Cord Are Significantly Higher in ICV-Treated Mice Than IV-Treated Mice

A potential explanation for the variable degree of rescue in the heart and hindlimb of IV-treated animals is based on potential differences in IGHMBP2 expression levels in cardiomyocytes versus the spinal cord. According to our results, the hindlimb function and distal muscle and NMJ phenotype were not sufficiently rescued in the IV-treated animals compared to ICV-treated animals. Therefore, we hypothesized that, due to the nature of IV injection, in which the virus enters the spinal cord through circulatory system as opposed to a direct delivery via ICV, the IGHMBP2 protein levels in the spinal cord of IV-treated mice is less than that of ICV-treated mice. We performed western blot analysis with the spinal cord extracts of IV- and ICV-injected *nmd* mice 12 days post-injection. As anticipated, IGHMBP2 protein levels were significantly higher in ICV-treated spinal cord extract compared to IV-treated and untreated mice (Figures 8A and 8B), elucidating the lack of sufficient repair in distal muscles of IV-injected mice. Since the heart of IV- and ICV-treated animals were rescued to the same extent, we assumed that the expression of IGHMBP2 was similar in the heart of IV and ICV-injected *nmd* mice. However, we failed to detect the appropriate size of the full-length IGHMBP2 protein in any of the heart samples at 12 days post-injection, which is in compliance with a previous report.[16] The main product of the western blot using heart extracts was a 55–60 kDa protein that was detected with similar intensity in all of the samples. This product has been previously suggested to originate from putative alternative splicing or an additional start codon.[16]

The absence of IGHMBP2 protein in the heart extracts prompted us to examine the full-length IGHMBP2 in a positive control *nmd* mouse. Therefore, we used the heart extracts of the cardiac rescue

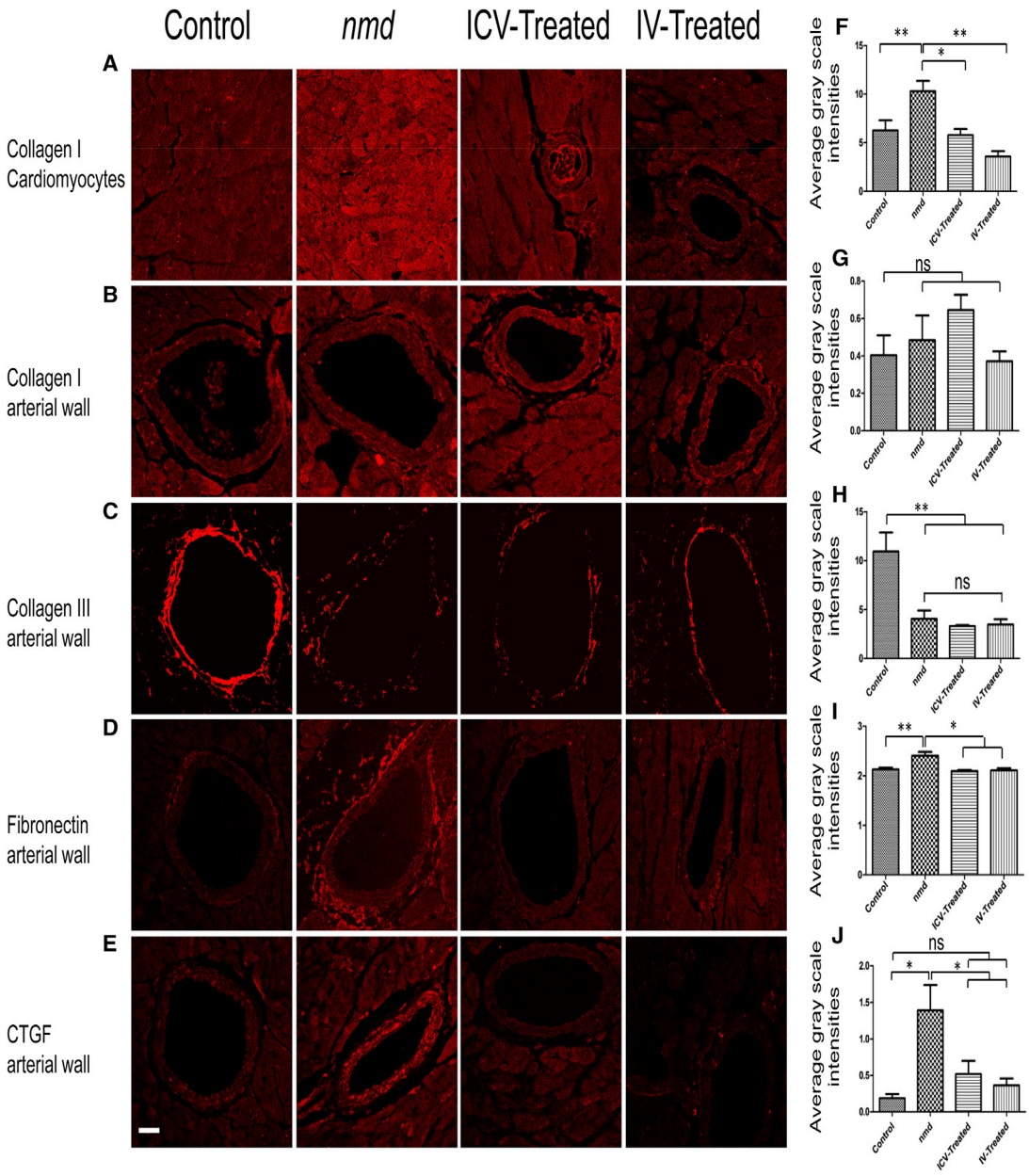

Figure 6. IV and ICV Treatments Rescue the Excess of ECM Proteins and Upregulation of CTGF

Representative confocal fluorescent images of heart sections in 8-week-old *nmd* males immunostained with collagen type I in cardiomyocytes (A) and arteries (B), collagen type III (C), fibronectin (D), and CTGF (E). (F) Quantification of collagen type I in cardiomyocytes shows a significant reduction in IV- and ICV-treated mice compared to untreated mice (one-way ANOVA, IV versus untreated, $p < 0.01$; ICV versus untreated, $p < 0.05$). (G and H) Quantification of collagen type I (G) and III (H) in arteries indicates no significant difference between IV- and ICV-treated mice compared to untreated mice, but healthy control mice contain a noticeably higher expression of collagen type III in arteries compared to treated and untreated *nmd* mice (one-way ANOVA, $p < 0.01$). (I and J) Quantification of fibronectin (I) and CTGF (J) in arteries demonstrates that the expression levels of these proteins are drastically reduced in both treated groups compared to the untreated group (one-way ANOVA, $p < 0.05$) and is similar to the healthy control group. Error bars represent mean ± SEM. Scale bars, 50 μm. *$p < 0.05$ and **$p < 0.01$.

transgenic line, constructed in Jackson Laboratory, that expresses IGHMBP2 in myocytes.[19] Interestingly, the full-length IGHMBP2 protein was barely detectable in the hearts of the transgenic heterozygous mice, as shown by a faint band, and almost undetectable in transgenic *nmd* mice, indicating that IGHMBP2 protein in the heart is not readily detectable or persistent (Figure S3). As expected, the 55–60 kDa protein was present in both transgenic and non-transgenic heart samples (Figure S3).

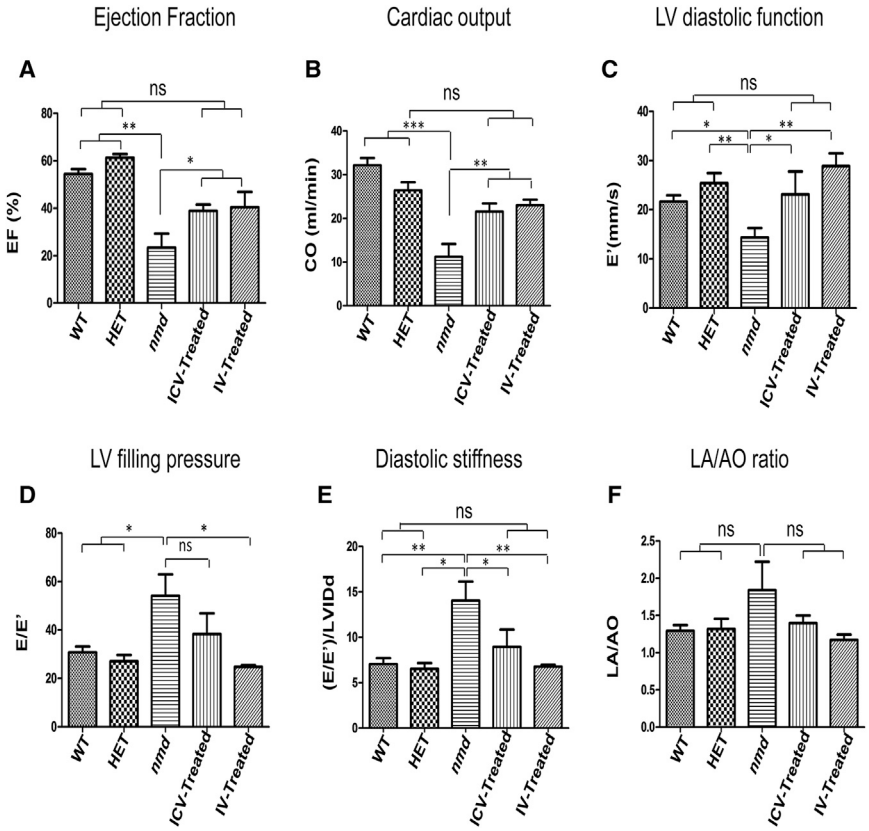

Figure 7. Cardiac Function of IV- and ICV-Treated SMARD1 Mice Are Equally Repaired Compared to Untreated Mice

Echocardiography was conducted on 8-week-old IV- and ICV-treated *nmd* males and compared to those of age-matched untreated and healthy controls (wild-type and "HET"). Untreated and wild-type (n = 5): "HET", IV- and ICV-treated (n = 4). Cardiac functional parameters, including ejection fraction, cardiac output, diastolic function, LV filling pressure, diastolic stiffness, and LA/AO ratio, were obtained using measurements from the modified parasternal short axis view in the M-mode. (A) Ejection fraction (one-way ANOVA, IV and ICV versus untreated, $p < 0.05$; IV and ICV versus "WT", ns; "WT" and "HET" versus untreated, $p < 0.001$). (B) Cardiac output (one-way ANOVA, IV and ICV versus untreated, $p < 0.01$; IV and ICV versus "HET", ns; "WT" versus IV and ICV, $p < 0.05$; "WT" and "HET" versus untreated, $p < 0.001$). (C) LV diastolic function (one-way ANOVA, IV and "HET" versus untreated, $p < 0.01$; ICV and "WT" versus untreated, $p < 0.05$; IV and ICV versus "WT" and "HET", ns). (D) LV filling pressure (one-way ANOVA, IV versus untreated, $p < 0.05$; "WT" and "HET" versus IV and ICV, ns; "WT" and "HET" versus untreated, $p < 0.05$; ICV versus untreated, ns). (E) Diastolic stiffness (one-way ANOVA, IV versus untreated, $p < 0.01$; ICV versus untreated, $p < 0.05$; IV and ICV versus "WT" and "HET", ns; "WT" versus untreated, $p < 0.01$; "HET" versus untreated, $p < 0.05$). (F) LA/AO ratio (one-way ANOVA, no significance between all groups). LA, lumen; AO, aorta. Error bars represent mean ± SEM. *$p < 0.05$, **$p < 0.01$, and ***$p < 0.001$.

DISCUSSION

Proper dosing, the therapeutic window, and the most effective delivery route are important components of pre-clinical studies for gene therapy. Two recent reports of gene replacement therapy for SMARD1 involved ICV delivery using two different doses[18] and IV delivery using a single high dose.[21] The outcome of the ICV delivery of a low dose[18] and the IV delivery of an approximately 5 times higher dose[21] was similar, leading to a significant phenotypic rescue. Since a sub-optimal dose can readily reveal even the minor differences between two delivery methods, we directly compared the efficacy of IV and ICV routes side by side using a low dose of AAV9-*IGHMBP2* (1.25e11 vg). In a direct comparison of IV- and ICV-treated animals, we observed that the injection method plays a critical role in influencing the type of tissues that are rescued. Our results indicate that delivery of a low dose vector through either IV or ICV is effective in extending the lifespan of *nmd* mice. Both delivery methods also led to significantly increased weight compared to untreated mice, although ICV-treated mice gained more weight than IV-treated mice. However, the IV delivery of the vector had a limited capability to repair the gastrocnemius muscles and NMJ phenotype, consistent with their poor rotarod performance, partial rescue of hindlimb contracture, and reduced activity level. Western blot with the spinal cord of IV- and ICV-treated mice revealed that the IGHMBP2 levels were significantly less in IV-treated spinal cord extracts than those treated by ICV injection, consistent with the inadequate rescue in IV-treated hindlimbs. The hindlimb phenotype of IV-treated mice was similar to untreated counterparts, confirming that progressive motor neuron disease, which leads to denervated NMJs and disabled distal muscles, is not the cause of death in *nmd* mice.

Dilated cardiomyopathy (DCM) occurs within 6 weeks of age in *nmd* mice.[19] Our cardiac analysis demonstrated that untreated *nmd* mice are harboring structural and cellular defects in the form of cardiomyocyte degeneration and interstitial and periarterial fibrosis. However, the cardiomyocytes of IV- and ICV-treated mice mostly resembled the healthy controls demonstrating normal myofiber area and a low level of interstitial and periarterial fibrosis. The biomarkers of fibrosis, such as excess ECM proteins and CTGF, were also drastically reversed in cardiomyocytes and the arteries of both IV- and ICV-injected animals compared to untreated animals, suggesting that fibrosis in *nmd* hearts is the result of CTGF upregulation leading to excessive ECM synthesis. Consistent with cellular repair, the echocardiography confirmed that the functional properties of IV- and ICV-treated mice are greatly improved to the level that several parameters, including ejection fraction, cardiac output, diastolic stiffness, and LV filling pressure, were not significantly different than healthy controls. On the other hand, the hearts of untreated *nmd* mice indicated impaired cardiac capacity and function,

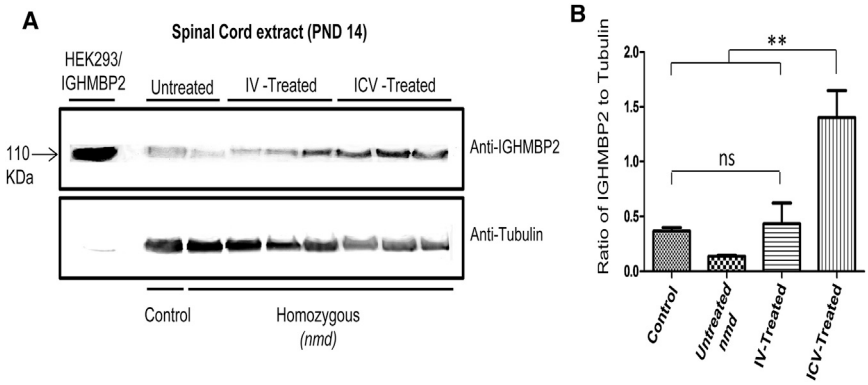

Figure 8. IGHMBP2 Protein Levels Are Higher in the Spinal Cord of ICV-Treated *nmd* Mice Than IV-Treated Mice

(A) Western blot of the spinal cord extracts of untreated and IV- and ICV-treated *nmd* mice 12 days post-injection. (B) Quantification of the western blot demonstrates a considerable increase in IGHMBP2 levels of ICV-treated mice compared to healthy control, untreated *nmd*, and IV-treated mice (one-way ANOVA, $p < 0.01$). Healthy control was utilized as positive control; HEK293 cells transfected with *IGHMBP2* construct was used as size control and anti-tubulin was used as loading control. Error bars represent mean ± SEM. $^{**}p < 0.01$.

even though only the untreated mice with stronger hearts were able to endure the anesthesia.

Cardiac improvement seen in the IV treatment group is potentially due to its effectiveness in restoring IGHMBP2 levels in the cardiomyocytes compared to the spinal cord. The cardiac repair in ICV-treated animals may be attributed to the immature blood-brain barrier at P2 that allows the transmission of the virus to peripheral organs, including cardiac tissue. However, neither western blot nor immunohistochemistry could reproducibly detect the predicted intracellular increases in IGHMBP2. IGHMBP2 is essentially undetectable in peripheral organs, including heart and liver, even at embryonic stage.[16] It is possible that delivery of a low dose of AAV9 vector is unable to increase the IGHMBP2 protein to a detectable level by western blot but is still sufficient to repair the cellular and functional properties of the heart. There is also a prominent 55–60 kDa truncated protein in all of the heart samples, including the cardiac rescue transgenic *nmd*, that may interfere with detection of the full-length IGHMBP2. We conclude that, although IV delivery of a low dose of AAV9-*IGHMBP2* has no positive outcome on hindlimb phenotype and function, partial restoration of cardiac structural and functional defects by IV delivery is sufficient to significantly rescue survival.

Our results are in agreement with the findings of cardiac rescue transgenic *nmd* mice in which introducing the full-length *Ighmbp2* cDNA under control of mouse titin (*Ttn*) promoter, expressed specifically in myocytes, increased the survival up to 8-fold.[19] In addition, three CAST-derived cardiac modifiers were identified by quantitative trait locus (QTL) on chromosomes 9, 10, and 16 of *nmd* mice with the ability to suppress symptoms of cardiomyopathy and extend the lifespan either individually or in combination.[19] The data provided in this report are consistent with these studies and further demonstrate that premature death in *nmd* mice occurs as a result of DCM, not progressive motor neuron disease. A similar degree of structural repair was also observed in the diaphragm of IV- and ICV-treated mice, which potentially contributed to extension of survival.

The fact that cardiomyopathy has not been reported in SMARD1 patients does not exclude the possibility of cardiac complications later in life because it occurs in congenital myopathies and muscular dystrophies.[33] The development of SMARD1-specific therapeutics has the potential to extend survival and, in turn, unmask currently unrecognized disease complications, such as cardiac defects. In SMA, even though the cardiac complications are limited to the most severe forms of disease, uncovering the defects in the heart and other peripheral organs of SMA mice models revealed the necessity of rescuing peripheral organs to achieve the full therapeutic potential for any treatment option.[30–32,34,35] Therefore, while cardiac defects have not been shown to be the cause of death in SMARD1 patients, these results highlight the importance of fully understanding the pathology of animal models and leveraging their strengths to investigate different components of gene therapy. Going forward, it will be important to examine the temporal requirements of AAV9 gene therapy and how an optimized delivery paradigm can be used to better address the temporal requirements of the AAV9-*IGHMBP2* vector.

MATERIALS AND METHODS

Viral Vector Construction

The vector expressing the full-length *IGHMBP2* cDNA was developed into the single-stranded AAV9 virus using an appropriate packaging cell line, purified by three CsCl density-gradient ultracentrifugation steps, and dialyzed against HEPES buffer. Viral particles were titered by qPCR using SYBR Green. The details of cloning and synthesis of single-stranded AAV9-*IGHMBP2* vector were described previously.[18]

Mice Model and Animal Procedures

All animal experiments took place in accordance with procedures approved by NIH guidelines and the University of Missouri (MU) Animal Care and Use Committee. A colony of the SMARD1 mice model (*nmd*) (B6.BKS*Ighmbp2nmd-2J*/J) (Jackson Laboratories, Bar Harbor, ME) has been established. The *nmd* mice were ICV[18] or IV injected[36] with 1.25×10^{11} vg at P2 and P3 for ICV injection[18] and at P2 for IV injection. For NMJ analysis of distal muscles, 4 groups of *nmd* mice (healthy controls [WT], untreated homozygous, ICV-treated, and IV-treated [n of 4 per each group]) were anesthetized with 2.5% isoflurane and then perfused transcardially with cold 0.1 M PBS (pH 7.4), followed by 4% paraformaldehyde in phosphate

buffer (0.1 M, pH 7.4). Diaphragm muscles were harvested from perfused animals for histopathology. For hindlimb and heart analysis, 4 treatment groups were anesthetized with 2.5% isoflurane, and their hindlimbs and hearts were incised and fixed in 4% paraformaldehyde overnight.

Contracture and Motor Function Test

Contracture was measured by placing the mice upside down in a conical tube and measuring the distance between the splayed hindlimbs. Motor activity and coordination were quantified using rotarod treadmill (IITC Rotarod Series 8, IITC Life Science, CA) with the speed of 5 rotations per minute. The animals were placed on textured drums to avoid slipping. When the tested animal fell onto the individual sensing platform, the test results were recorded in seconds. For forelimb grip strength measurement, a grasping response test was utilized. Each pup's front paws were placed on a wire mesh (1 cm^2 grids) and gently dragged horizontally along the mesh (BioSeb Model BP32025; Vitrolles, FR, EU, Pinellas Park, FL). Any resistance felt was scored as a positive response. The strength of the animal holding onto the mesh before release was recorded in grams. Grip strength values (gram) were normalized against the animal's body weight. Both measurements were performed for 7 alternate days, starting on P50 and ending at P62. Each value is the average of four trials performed on each day.

Muscle Histology

4 μm VVG-stained cross sections were prepared from gastrocnemius, diaphragm, and heart muscles at the MU Veterinary Medical Diagnostic Laboratory. Muscle fiber area and interstitial and periarterial fibrosis were quantified using MetaVue as previously described.[18,30,37]

Neuromuscular Junction Immunostaining

This procedure was described in detail previously.[38] In summary, gastrocnemius muscles were harvested from 8 week-old-perfused mice and teased into bundles of 10–15 muscle fibers to promote the penetration of antibodies. Muscles were immunostained using anti-NF-H (1:2,000; Chemicon, EMD Millipore) and anti-synaptophysin (1:200; Life Technologies). Acetylcholine receptors were labeled with Alexa Fluor 594-conjugated α-bungarotoxin (1:200; Life Technologies). Representative muscle images were taken using a laser scanning confocal microscope (×40 objective; Leica TCS SP8, Leica Microsystems). NMJ analysis was performed on at least 3 randomly selected fields of view per muscle per mouse (×20 objective; Leica DM5500 B, Leica Microsystems). Images were analyzed using freely available Fiji Software (NIH). Endplates missing overlapping nerve terminal staining were considered completely denervated. Endplates with partial overlap were considered partially denervated, and endplates with complete overlap were considered fully innervated. Endplate morphology was assessed for normal (pretzel shape) or fragmented structure.

Cardiac Ultrasound

To evaluate the cardiac function of *nmd* mice *in vivo*, we performed echocardiography on 8-weeks-old isoflurane-anesthetized males using a Vevo 2100 ultrasound system (VisualSonics, Toronto, Canada) as previously described.[39] Qualitative and quantitative measurements were analyzed offline using the Vevo software.

Western Blot

100 mg spinal cord and heart tissue were homogenized in 200–500 μL Jurkat lysis buffer (JLB) and equal amounts of protein were loaded onto 10% SDS-PAGE gel as previously described.[37,40,41] Blots were incubated overnight at 4°C with rabbit IGHMBP2 antibody (Aviva Systems Biology, San Diego, CA) diluted to 1:1,000, and horseradish peroxidase (HRP) anti-rabbit immunoglobulin G (IgG) (Jackson Immunoresearch) was used as secondary antibody. Mouse tubulin (Sigma, St. Louis, MO) was used as loading control. Blots were visualized by chemiluminescence, and images were captured by a Fugi-Imager (LAS-3000) and quantified by Multi Gauge V3.0 software.

Heart Immunohistochemistry

Immunostaining of the cardiomyocytes and vasculature was previously described in detail.[30,37] Paraffin-embedded heart crosssections were immuno-labeled for rabbit collagen I (1:100), collagen III (1:50), CTGF (1:300), TGFβ1 (1:50), and fibronectin (1:50). All antibodies were purchased from Abcam. 1:300 dilution of Alexa Fluor 647 donkey anti-rabbit IgG (H+L) (Invitrogen) was used as secondary antibody. Cardiomyocytes were also stained with 10 μg/mL FITC-tagged wheat germ agglutinin (Invitrogen). Images were captured using an inverted spectral confocal microscope (Leica TCP SP8 STED) under the same computer settings for all sections in each experiment. The cross-sectional area of myocytes and gray scale intensities in cardiomyocytes and coronary arteries were measured by MetaVue and MetaMorph.

Statistical Analysis

The statistical significance of comparing three experimental groups (healthy control, untreated, and ICV- and IV-treated) in all the experiments was calculated using one-way ANOVA and Newman-Keuls multiple comparison post hoc test. Analyses were performed with GraphPad Prism software; error bars represent means ± SEM. The significance of survival was determined with a log-ranked (Mantel-Cox) test. Ratios were calculated as values from controls ("HET" or "WT") standardized as 1.

SUPPLEMENTAL INFORMATION

Supplemental Information includes three figures and can be found with this article online at https://doi.org/10.1016/j.omtm.2018.08.005.

AUTHOR CONTRIBUTIONS

M.S. and C.L.L. designed the experiments and wrote and edited the manuscript. M.S., E.V., K.A.K., and V.D. conducted the experiments.

CONFLICTS OF INTEREST

All authors except C.L.L. declare no competing financial interests. C.L.L. is the co-founder and Chief Scientific Officer of Shift Pharmaceuticals.

ACKNOWLEDGMENTS

We would like to thank Kyra Florea, Madeline Simon, Siri O'Day, and Mona Garro for technical assistance. We greatly appreciate Dr. Amy N. Hicks and Dr. Gregory A. Cox at Jackson Laboratory for their generous gift of the cardiac rescue transgenic *nmd* mice. We are grateful for the services rendered by the MU Molecular Cytology Core, Veterinary Medical Diagnostic Laboratory, and resources and facilities at the Harry S. Truman Memorial Veterans Hospital, including the Small Animal Ultrasound Imaging Center (ultrasound). The authors would also like to thank SMA Europe for previous funding support leading up to this project. This work is supported by NIH/NINDS grant R21NS093175 (to C.L.L. and M.S.) and the Sims' Fund to Cure SMARD (to M.S.).

REFERENCES

1. Grohmann, K., Varon, R., Stolz, P., Schuelke, M., Janetzki, C., Bertini, E., Bushby, K., Muntoni, F., Ouvrier, R., Van Maldergem, L., et al. (2003). Infantile spinal muscular atrophy with respiratory distress type 1 (SMARD1). Ann. Neurol. *54*, 719–724.
2. Rudnik-Schöneborn, S., Stolz, P., Varon, R., Grohmann, K., Schächtele, M., Ketelsen, U.P., Stavrou, D., Kurz, H., Hübner, C., and Zerres, K. (2004). Long-term observations of patients with infantile spinal muscular atrophy with respiratory distress type 1 (SMARD1). Neuropediatrics *35*, 174–182.
3. Grohmann, K., Wienker, T.F., Saar, K., Rudnik-Schöneborn, S., Stoltenburg-Didinger, G., Rossi, R., Novelli, G., Nürnberg, G., Pfeufer, A., Wirth, B., et al. (1999). Diaphragmatic spinal muscular atrophy with respiratory distress is heterogeneous, and one form Is linked to chromosome 11q13-q21. Am. J. Hum. Genet. *65*, 1459–1462.
4. Grohmann, K., Schuelke, M., Diers, A., Hoffmann, K., Lucke, B., Adams, C., Bertini, E., Leonhardt-Horti, H., Muntoni, F., Ouvrier, R., et al. (2001). Mutations in the gene encoding immunoglobulin mu-binding protein 2 cause spinal muscular atrophy with respiratory distress type 1. Nat. Genet. *29*, 75–77.
5. Lim, S.C., Bowler, M.W., Lai, T.F., and Song, H. (2012). The Ighmbp2 helicase structure reveals the molecular basis for disease-causing mutations in DMSA1. Nucleic Acids Res. *40*, 11009–11022.
6. Viollet, L., Barois, A., Rebeiz, J.G., Rifai, Z., Burlet, P., Zarhrate, M., Vial, E., Dessainte, M., Estournet, B., Kleinknecht, B., et al. (2002). Mapping of autosomal recessive chronic distal spinal muscular atrophy to chromosome 11q13. Ann. Neurol. *51*, 585–592.
7. Fukita, Y., Mizuta, T.R., Shirozu, M., Ozawa, K., Shimizu, A., and Honjo, T. (1993). The human S mu bp-2, a DNA-binding protein specific to the single-stranded guanine-rich sequence related to the immunoglobulin mu chain switch region. J. Biol. Chem. *268*, 17463–17470.
8. de Planell-Saguer, M., Schroeder, D.G., Rodicio, M.C., Cox, G.A., and Mourelatos, Z. (2009). Biochemical and genetic evidence for a role of IGHMBP2 in the translational machinery. Hum. Mol. Genet. *18*, 2115–2126.
9. Guenther, U.P., Handoko, L., Laggerbauer, B., Jablonka, S., Chari, A., Alzheimer, M., Ohmer, J., Plöttner, O., Gehring, N., Sickmann, A., et al. (2009). IGHMBP2 is a ribosome-associated helicase inactive in the neuromuscular disorder distal SMA type 1 (DSMA1). Hum. Mol. Genet. *18*, 1288–1300.
10. Molnar, G.M., Crozat, A., Kraeft, S.K., Dou, Q.P., Chen, L.B., and Pardee, A.B. (1997). Association of the mammalian helicase MAH with the pre-mRNA splicing complex. Proc. Natl. Acad. Sci. USA *94*, 7831–7836.
11. Chen, N.N., Kerr, D., Chang, C.F., Honjo, T., and Khalili, K. (1997). Evidence for regulation of transcription and replication of the human neurotropic virus JCV genome by the human S(mu)bp-2 protein in glial cells. Gene *185*, 55–62.
12. Miao, M., Chan, S.L., Fletcher, G.L., and Hew, C.L. (2000). The rat ortholog of the presumptive flounder antifreeze enhancer-binding protein is a helicase domain-containing protein. Eur. J. Biochem. *267*, 7237–7246.
13. Zhang, Q., Wang, Y.C., and Montalvo, E.A. (1999). Smubp-2 represses the Epstein-Barr virus lytic switch promoter. Virology *255*, 160–170.
14. Cox, G.A., Mahaffey, C.L., and Frankel, W.N. (1998). Identification of the mouse neuromuscular degeneration gene and mapping of a second site suppressor allele. Neuron *21*, 1327–1337.
15. Cook, S.A., Johnson, K.R., Bronson, R.T., and Davisson, M.T. (1995). Neuromuscular degeneration (nmd): a mutation on mouse chromosome 19 that causes motor neuron degeneration. Mamm. Genome *6*, 187–191.
16. Grohmann, K., Rossoll, W., Kobsar, I., Holtmann, B., Jablonka, S., Wessig, C., Stoltenburg-Didinger, G., Fischer, U., Hübner, C., Martini, R., and Sendtner, M. (2004). Characterization of Ighmbp2 in motor neurons and implications for the pathomechanism in a mouse model of human spinal muscular atrophy with respiratory distress type 1 (SMARD1). Hum. Mol. Genet. *13*, 2031–2042.
17. Krieger, F., Elflein, N., Saenger, S., Wirthgen, E., Rak, K., Frantz, S., Hoeflich, A., Toyka, K.V., Metzger, F., and Jablonka, S. (2014). Polyethylene glycol-coupled IGF1 delays motor function defects in a mouse model of spinal muscular atrophy with respiratory distress type 1. Brain *137*, 1374–1393.
18. Shababi, M., Feng, Z., Villalon, E., Sibigtroth, C.M., Osman, E.Y., Miller, M.R., Williams-Simon, P.A., Lombardi, A., Sass, T.H., Atkinson, A.K., et al. (2016). Rescue of a Mouse Model of Spinal Muscular Atrophy With Respiratory Distress Type 1 by AAV9-IGHMBP2 Is Dose Dependent. Mol. Ther. *24*, 855–866.
19. Maddatu, T.P., Garvey, S.M., Schroeder, D.G., Zhang, W., Kim, S.Y., Nicholson, A.I., Davis, C.J., and Cox, G.A. (2005). Dilated cardiomyopathy in the nmd mouse: transgenic rescue and QTLs that improve cardiac function and survival. Hum. Mol. Genet. *14*, 3179–3189.
20. Maddatu, T.P., Garvey, S.M., Schroeder, D.G., Hampton, T.G., and Cox, G.A. (2004). Transgenic rescue of neurogenic atrophy in the nmd mouse reveals a role for Ighmbp2 in dilated cardiomyopathy. Hum. Mol. Genet. *13*, 1105–1115.
21. Nizzardo, M., Simone, C., Rizzo, F., Salani, S., Dametti, S., Rinchetti, P., Del Bo, R., Foust, K., Kaspar, B.K., Bresolin, N., et al. (2015). Gene therapy rescues disease phenotype in a spinal muscular atrophy with respiratory distress type 1 (SMARD1) mouse model. Sci. Adv. *1*, e1500078.
22. Burge, C., Tuschl, T., and Sharp, P. (1999). Splicing of precursors to mRNAs by the splicesomes. The RNA world (New York: Cold Spring Harbor Laboratory Press Cold Spring Harbor), pp. 525–560.
23. Fan, D., Takawale, A., Lee, J., and Kassiri, Z. (2012). Cardiac fibroblasts, fibrosis and extracellular matrix remodeling in heart disease. Fibrogenesis Tissue Repair *5*, 15.
24. Szabó, Z., Magga, J., Alakoski, T., Ulvila, J., Piuhola, J., Vainio, L., Kivirikko, K.I., Vuolteenaho, O., Ruskoaho, H., Lipson, K.E., et al. (2014). Connective tissue growth factor inhibition attenuates left ventricular remodeling and dysfunction in pressure overload-induced heart failure. Hypertension *63*, 1235–1240.
25. Borthwick, L.A., Wynn, T.A., and Fisher, A.J. (2013). Cytokine mediated tissue fibrosis. Biochim. Biophys. Acta *1832*, 1049–1060.
26. Campbell, S.E., and Katwa, L.C. (1997). Angiotensin II stimulated expression of transforming growth factor-beta1 in cardiac fibroblasts and myofibroblasts. J. Mol. Cell. Cardiol. *29*, 1947–1958.
27. Chen, C.C., and Lau, L.F. (2009). Functions and mechanisms of action of CCN matricellular proteins. Int. J. Biochem. Cell Biol. *41*, 771–783.
28. Frangogiannis, N.G. (2012). Matricellular proteins in cardiac adaptation and disease. Physiol. Rev. *92*, 635–688.
29. Way, K.J., Isshiki, K., Suzuma, K., Yokota, T., Zvagelsky, D., Schoen, F.J., Sandusky, G.E., Pechous, P.A., Vlahos, C.J., Wakasaki, H., and King, G.L. (2002). Expression of connective tissue growth factor is increased in injured myocardium associated with protein kinase C beta2 activation and diabetes. Diabetes *51*, 2709–2718.
30. Shababi, M., Habibi, J., Yang, H.T., Vale, S.M., Sewell, W.A., and Lorson, C.L. (2010). Cardiac defects contribute to the pathology of spinal muscular atrophy models. Hum. Mol. Genet. *19*, 4059–4071.
31. Heier, C.R., Satta, R., Lutz, C., and DiDonato, C.J. (2010). Arrhythmia and cardiac defects are a feature of spinal muscular atrophy model mice. Hum. Mol. Genet. *19*, 3906–3918.
32. Bevan, A.K., Hutchinson, K.R., Foust, K.D., Braun, L., McGovern, V.L., Schmelzer, L., Ward, J.G., Petruska, J.C., Lucchesi, P.A., Burghes, A.H., and Kaspar, B.K. (2010). Early heart failure in the SMNDelta7 model of spinal muscular atrophy and correction by postnatal scAAV9-SMN delivery. Hum. Mol. Genet. *19*, 3895–3905.

33. Finsterer, J., and Stöllberger, C. (2000). Cardiac involvement in primary myopathies. Cardiology *94*, 1–11.

34. Shababi, M., Lorson, C.L., and Rudnik-Schöneborn, S.S. (2014). Spinal muscular atrophy: a motor neuron disorder or a multi-organ disease? J. Anat. *224*, 15–28.

35. Hamilton, G., and Gillingwater, T.H. (2013). Spinal muscular atrophy: going beyond the motor neuron. Trends Mol. Med. *19*, 40–50.

36. Glascock, J.J., Osman, E.Y., Coady, T.H., Rose, F.F., Shababi, M., and Lorson, C.L. (2011). Delivery of therapeutic agents through intracerebroventricular (ICV) and intravenous (IV) injection in mice. J. Vis. Exp. Published online October 3, 2011. https://doi.org/10.3791/2968.

37. Shababi, M., Habibi, J., Ma, L., Glascock, J.J., Sowers, J.R., and Lorson, C.L. (2012). Partial restoration of cardio-vascular defects in a rescued severe model of spinal muscular atrophy. J. Mol. Cell. Cardiol. *52*, 1074–1082.

38. Villalón, E., Shababi, M., Kline, R., Lorson, Z.C., Florea, K.M., and Lorson, C.L. (2018). Selective vulnerability in neuronal populations in nmd/SMARD1 mice. Hum. Mol. Genet. *27*, 679–690.

39. Habibi, J., Aroor, A.R., Sowers, J.R., Jia, G., Hayden, M.R., Garro, M., Barron, B., Mayoux, E., Rector, R.S., Whaley-Connell, A., and DeMarco, V.G. (2017). Sodium glucose transporter 2 (SGLT2) inhibition with empagliflozin improves cardiac diastolic function in a female rodent model of diabetes. Cardiovasc. Diabetol. *16*, 9.

40. Shababi, M., Glascock, J., and Lorson, C.L. (2011). Combination of SMN trans-splicing and a neurotrophic factor increases the life span and body mass in a severe model of spinal muscular atrophy. Hum. Gene Ther. *22*, 135–144.

41. Shababi, M., and Lorson, C.L. (2012). Optimization of SMN trans-splicing through the analysis of SMN introns. J. Mol. Neurosci. *46*, 459–469.

OMTM, Volume *10*

Supplemental Information

A Direct Comparison of IV and ICV Delivery Methods for Gene Replacement Therapy in a Mouse Model of SMARD1

Monir Shababi, Eric Villalón, Kevin A. Kaifer, Vince DeMarco, and Christian L. Lorson

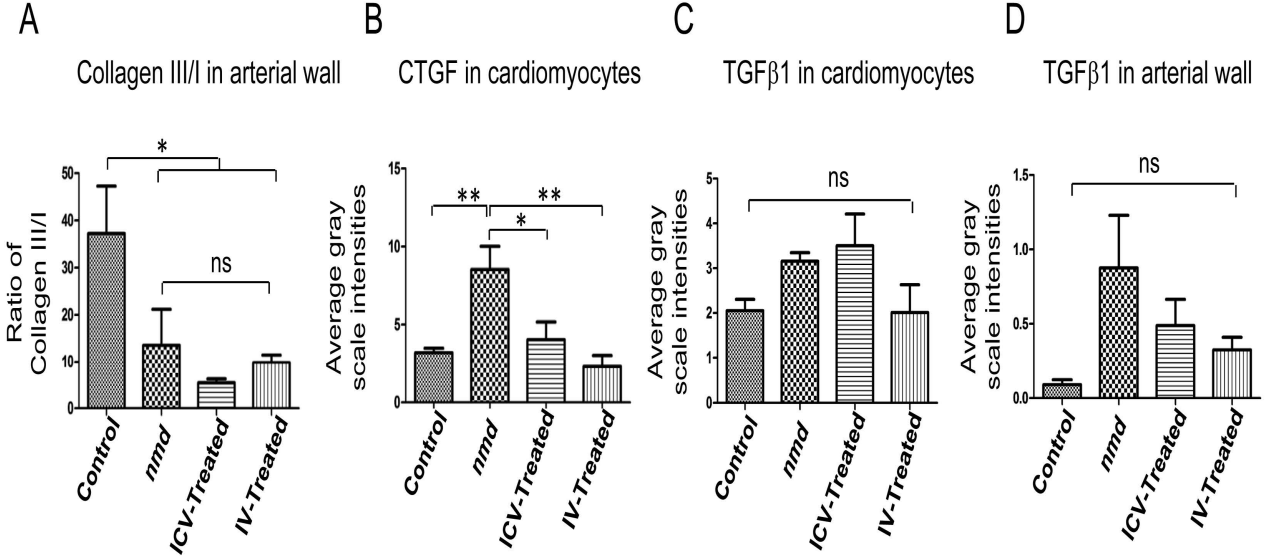
A
Collagen III/I in arterial wall
Ratio of Collagen III/I
50
40
30
20
10
0
*
ns
Control
nmd
ICV-Treated
IV-Treated
B
CTGF in cardiomyocytes
Average gray scale intensities
15
10
5
0
**
**
*
Control
nmd
ICV-Treated
IV-Treated
C
TGFβ1 in cardiomyocytes
Average gray scale intensities
5
4
3
2
1
0
ns
Control
nmd
ICV-Treated
IV-Treated
D
TGFβ1 in arterial wall
Average gray scale intensities
1.5
1.0
0.5
0.0
ns
Control
nmd
ICV-Treated
IV-Treated

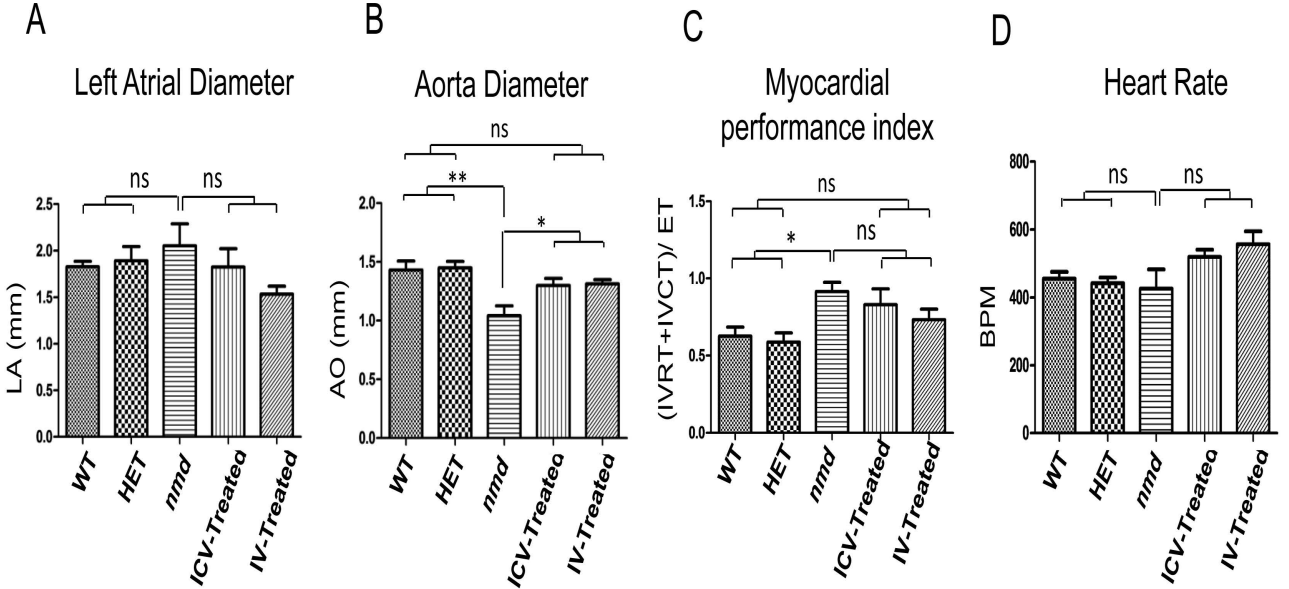
A
Left Atrial Diameter
LA (mm)
ns
ns
2.5
2.0
1.5
1.0
0.5
0.0
WT
HET
nmd
ICV-Treated
IV-Treated
B
Aorta Diameter
AO (mm)
ns
**
*
2.0
1.5
1.0
0.5
0.0
WT
HET
nmd
ICV-Treated
IV-Treated
C
Myocardial performance index
(IVRT+IVCT)/ ET
ns
*
ns
1.5
1.0
0.5
0.0
WT
HET
nmd
ICV-Treated
IV-Treated
D
Heart Rate
BPM
ns
ns
800
600
400
200
WT
HET
nmd
ICV-Treated
IV-Treated

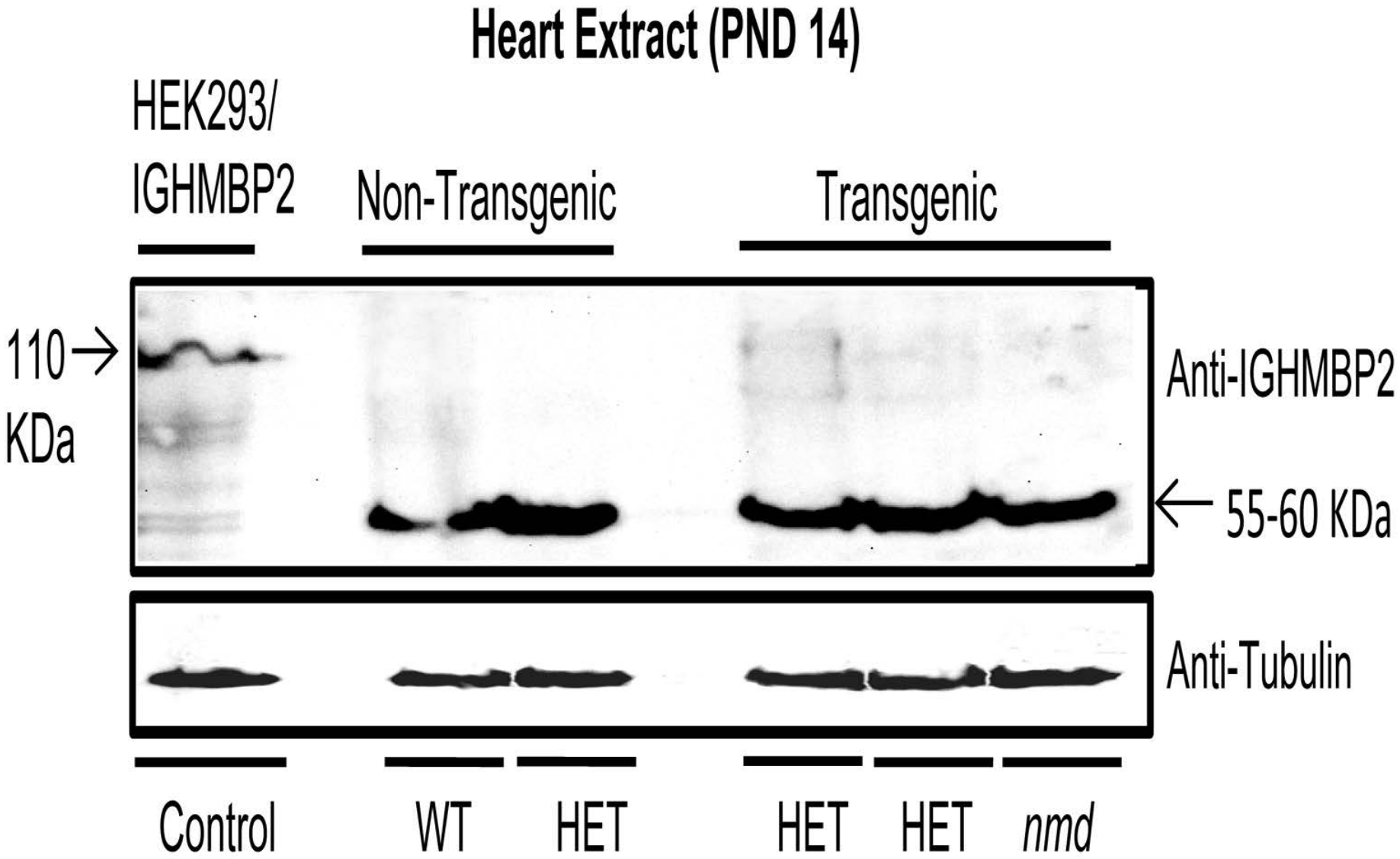
Heart Extract (PND 14)
HEK293/
IGHMBP2
Non-Transgenic
Transgenic
110→
KDa
Anti-IGHMBP2
← 55-60 KDa
Anti-Tubulin
Control
WT
HET
HET
HET
nmd

Figure S1. Expression levels of ECM proteins and growth factors in Cardiomyocytes and arteries of *nmd* heart. (**A**) Ratio of collagen III/I in arteries (one-way ANOVA unaffected control vs. *nmd*, IV, and ICV treated, $P< 0.05$); (**B**) Expression of CTGF in cardiomyocytes (one-way ANOVA IV-treated vs. *nmd*, $P<0.01$; ICV-treated vs. *nmd*, $P<0.05$) (**C**, **D**) expression of TGFβ in cardiomyocytes (**C**) and arteries (**D**). The levels of TGFβ are not significantly different between the cohorts.

Figure S2. Functional parameters of *nmd* heart. (**A**) Left atrial diameter; (**B**) Aorta diameter; (**C**) Myocardial performance index (one-way ANOVA controls vs. *nmd*, $P<0.05$); (**D**) Heart rate. BPM (beat per minute).

Figure S3. **Expression level of IGHMBP2 in cardiac rescue transgenic *nmd*.** Western blot with the heart extracts of non-transgenic and cardiac rescue transgenic *nmd* detects a low expression of IGHMBP2 in transgenic heart. HEK 293 cells transfected with IGHMBP2 construct was used as size control and anti-tubulin was used as loading control.